7 | APPENDIXES

7.1 | Time Resolved Absorption Measurements

7.2 | Mossbauer Spectroscopy

7.3 | Nonlinear Optical Measurements

7.1 | Time Resolved Absorption Measurements

Time resolved (or transient) absorption experiments provide a very powerful tool to study the intermediate states in a photo-induced reaction. Because of the very diverse time scales (seconds to femptoseconds) that can be involved in these processes usually different experimental setups have to be used. In our case, the nanosecond time scale setup it is has been probe to be not enough fast for our systems, while the (sub)picoseconds time scale set up would be the right one.

PICOSECOND TRANSIENT ABSORPTION SPECTROSCOPY

The results from the picosecond transient absorption measurements presented in Chapter 3.2 were obtained in the group of Prof. A.M. Brouwer at the University of Amsterdam. A schematic outline of their set-up is depicted in Figure 67.

The setup consists of a laser system based on a Spectra-Physics Hurricane Ti:Sapphire regenerative amplifier system. The optical bench assembly of the Hurricane includes a seeding laser (Mai Tai), a pulse stretcher, a Ti:Sapphire regenerative amplifier, a Q-switched pumped laser (Evolution) and a pulse compressor. The output of the laser is typically 1 mJ/pulse (fwhm = 130 fs) at a repetition rate of 1 kHz.

Two different pump-probe set-ups were used (see Figure 67): (i) A full spectrum setup based on an optical parametric amplifier (Spectra-Physics OPA 800) as pump and residual fundamental light (150 μ J/pulse) from the pump OPA used for white light generation and a CCD spectrometer as detector. (ii) Single wavelength kinetics measurements are based on the use of two OPAs, where one is used as pump and the other as probe, and an amplified Si-photo diode for detection (see Figure 67). For both set-ups the OPA was used to generate excitation pulses at 340 nm, typically 5 μ J/pulse (fourth harmonic of the 1360 nm OPA signal beam).

The white light generation was accomplished by focusing the fundamental (800 nm) into a water flow-through cell (10 mm, Hellma). For the single wavelength measurements, the polarization of probe light was controlled by a Berek Polarization Compensator (New Focus). The probe light was passed over a delay line (Physik Instrumente, M-531DD) that provides an experimental time window of 1.8 ns with a maximal resolution of 0.6 fs/step. The energy of the probe pulses was *ca.* 5×10^{-3} μJ/pulse at the sample. The angle between the pump and the probe beam is typically 7 - 10°. The circular holder (d = 1.8 cm; 1 mm, Hellma), with a solution of the sample, was placed in a home made rotating ball bearing (1000 rpm), avoiding local heating by the laser beams (Figure 68b). The solutions of the samples were prepared to have an optical density of *ca.* 0.8 over 1 mm at the excitation wavelength.

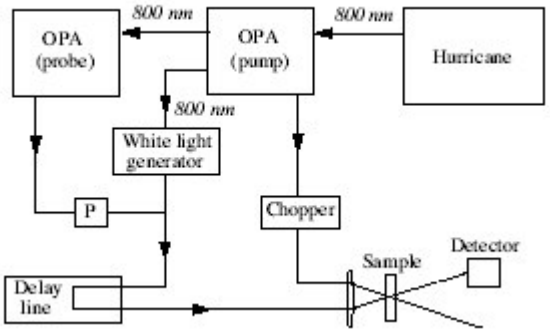

Figure 67. Schematic representation of the (sub)picosecond transient absorption setup P is a Berek polarizer and the detector can be a CCD (for spectra) or a Si-photo diode (for single line measurements).

For the white light/CCD set up, the probe beam was coupled into an optical fibre after passing the sample and coupled into a CCD spectrometer (Ocean Optics, PC2000). A chopper, placed in the excitation beam, provides I and I_0 depending on the status of the chopper (open or closed). Typically, 2000 excitation pulses were averaged to obtain the transient at a particular time. Due to the lenses a chirp of ~1 ps is observed between 460 - 650 nm.

For the single wavelength kinetic measurement, an amplified Si-photo diode (New-Port, 818UV / 4832-C) was used for detection. The output of the Si-photo diode, connected to an AD-converter (National Instruments, PCI 4451, 205 kS/s), enabled the measurement of the intensity of each separate pulse. Typically, 500 excitation pulses were averaged to obtain the transient absorption at a particular time.

(a)

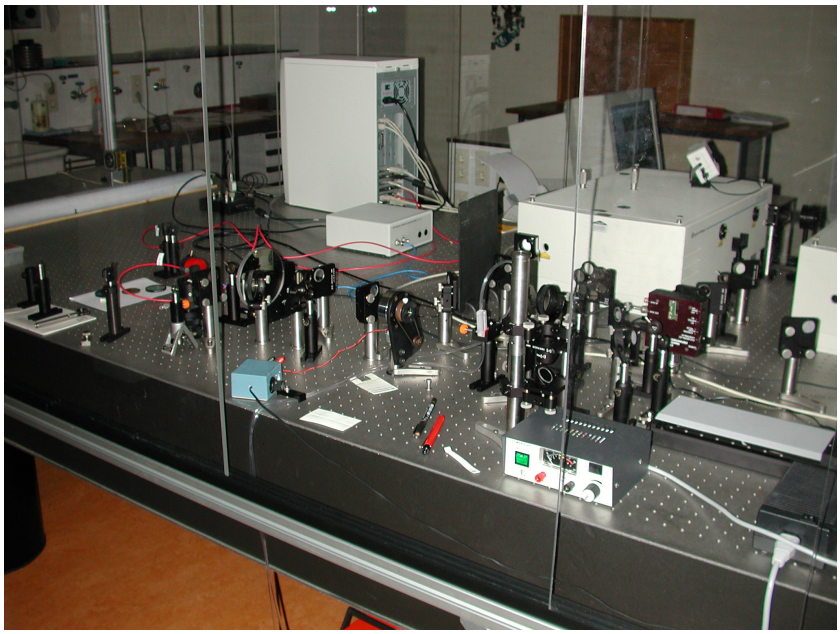

(b)

Figure 68. (a) Picture of the the set-up used for the picosecond transient absorption experiments in the laboratory of Prof. A. M. Brouwer at the University of Amsterdam, (b) Cell holder with fast rotation.

7.2 | Mössbauer Spectroscopy

7.2.1 INTRODUCTION

Mössbauer spectroscopy is used primarily to study the electron structure of materials. This technique is based in the fact that nuclear radiation can be emitted and absorbed recoilless if the atoms are placed in the solid state. For this experiment, also called nuclear resonant absorption, one needs a radioactive source which decays via an excited state into the so-called Mössbauer isotope. Depending on the lifetime of the excited state, the energy of the radiation can be extremely sharp. In the case of the ^{57}Fe isotope the energy uncertainty, called natural line width, is 5×10^{-9} eV compared to the energy of 14.4×10^{3} eV of the radiation. Because the energy of the nuclear state is so well defined, the difference between the hyperfine interaction of the isotopes in the source and the sample can be studied.

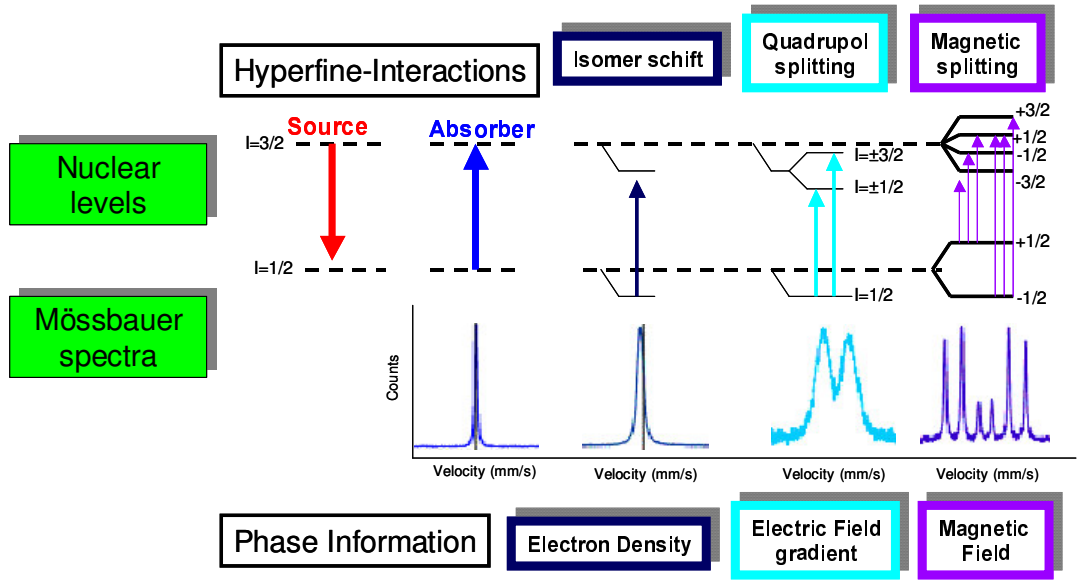

Scheme 32

The influence of the hyperfine interaction in the case of ^{57}Fe is shown in Scheme 32. The spectra resulting from these interactions are also shown. this They can be measured by moving the source. Via the Doppler-effect the energy increases if the source moves towards the sample and vice versa. A velocity of 1 mm/s corresponds to an energy of 50×10^{-9} eV.

Absorption can only occur, if the spectrum of the source overlaps with energy levels of the sample. Hence the Mössbauer spectrum is a picture of the hyperfine interaction of the sample. Several parameters can be extracted from the spectrum. These parameters can determine the chemical and magnetic phases of the sample like a fingerprint.

7.2.2 NUCLEAR PHYSICS OF Fe^{57}

The isotope with the strongest recoilless resonant absorption is Fe^{57}. Since the vast majority of the work reported in the Mössbauer literature is for iron, we restrict our discussion to that isotope. Of all the excited Fe^{57} nuclei, about 10% will emit a 14.4 keV gamma ray via a magnetic dipole transition from the metastable I = 3/2 state to the I = 1/2 ground state (I is the nuclear spin). The ratio of recoil-free 14.4 keV photons to all the 14.4 keV photons emitted is f, the recoil-free fraction of the source. f varies with the properties of the solid and decreases monotonically with increasing temperature. The linewidth of the emitted radiation is limited in theory by t, the mean life of the I = 3/2 state. In Fe^{57}, t = 1.4 x 10^{-7} sec, and the energy distribution is given by a Lorentzian with a fullwidth at half maximum of Γ_{nat} = 4.7 x 10^{-9} eV (Lang, 1970). The intensity per unit energy of the Mössbauer radiation is many orders of magnitude greater than the background radiation, and we shall henceforth refer to the gamma beam as if it were 100% Mössbauer radiation unless we specifically note otherwise. We shall also assume that the nuclear levels of the source are not split, and the energy distribution of the beam is given by a single Lorentzian.

To use our Mössbauer source as a spectroscopic tool we must be able to vary its energy over a significant range. This is accomplished by Doppler shifting the energy of the gamma beam. Moving the source at a velocity of 1 mm/sec toward the sample will increase the energy of the photons by 14.4 keV (v/c) = 4.8 x 10^{-8} eV or ten natural linewidths. The "mm/sec" is a convenient Mössbauer unit and is equal to 4.8 x 10^{-8} eV for Fe^{57}. A Mössbauer spectrometer consists of a source which may be moved relative to the sample and a counter to monitor the intensity of the beam after it has passed through the sample. The Mössbauer spectrum is a plot of the counting rate against the source velocity, i.e., the beam energy.

7.2.3 HYPERFINE INTERACTIONS

7.2.3.1. Isomer Shift

The nucleus and its electrons interact in several ways, the most obvious being the electrostatic attraction. If the Fe^{57} nuclear charge distribution were the same for the I = 1/2 ground state and the I = 3/2 excited state, then the electrostatic energy of the system of electrons plus nucleus would be the same for both states. In fact the excited Fe^{57} nucleus is 0.1% smaller in radius than the ground state nucleus, which causes the Mössbauer transition energy to depend on the electron density at the nucleus. This effect produces the so-called isomer shift of the Mössbauer spectrum (Scheme 32)

7.2.3.2. Electric Quadrupole Interaction

The excited (I = 3/2) state of the Fe^{57} nucleus possesses an electric quadrupole moment, and the presence of a low symmetry electric field will tend to orient the nuclear spin. Each orientation has a different energy so that this interaction originates a splitting of the energy levels. Reversal of the sign of the nuclear spin will not change the nuclear charge distribution. The quartet will be split into two doublets, while the I = 1/2 states will remain degenerate. Since two transition energies are now possible, two absorption peaks will appear in the Mössbauer spectrum (Scheme 32).

If the recoil-free fraction does not depend on the orientation of the γ-beam relative to the Fe site, a sample with randomly oriented sites in zero applied field will produce a symmetric quadrupole pair. Since the sign of the difference of the energy of the two peaks(ΔE) can not be determined from such a spectrum, the absolute value of ΔE is usually called "the quadrupole splitting."

7.2.3.3. Magnetic Hyperfine Interaction

The Fe^{57} nucleus possesses a magnetic moment and its energy levels are perturbed by the local magnetic field. In the presence of a field *H*, the interaction is

$$H^M = -g_N \beta N.I.H \qquad \text{Equation 19}$$

where β_N is the nuclear magneton and g_N is the nuclear gyromagnetic ratio. *H* will be the sum of an applied field with the internal field of the unpaired electrons. Depending on the magnetic properties of the sample, the internal field may or may not equal zero in the absence of the applied field (Scheme 32).

7.2.4. Experimental Set-Up

Since the hyperfine interaction cause small variation in the energy level structure, then the gamma energy emitted by the source doesn't correspond to the energy of the transition of the absorber material. Such energy difference is neutralized by the Doppler Effect by moving the source. In the case of the ^{57}Fe, the energy of the transition is 14.4 eV, and the velocity required to neutralize the hyperfine shifts are around mm/s.

The Mössbauer spectra are usually recorded in the transmission geometry using a constant acceleration spectrometer operated in connection with a multi-channel analyser in the time scale mode synchronized with the source velocity. Each velocity have a different channel. The source is kept at room temperature and consists of approximately 20 mCi of Co^{57} diffused into rhodium or palladium foil. The spectrometer is calibrated against a metallic iron foil and zero velocity is taken as the centroid of its room temperature

Mössbauer spectrum. In such calibration spectra, linewidths of about 0.23 mm/s were normally observed. Finally a double spectra is obtained (due to the fact that the velocity first increase and then decrease) . It is necessary to transform it to a single spectra. The experimental spectra it must be adjust to a lorenzian theoric spectra and if we have a good fit it is possible to have a lot of data about the electronic and magnetic configuration of the sample. The duration of a typical run is usually a few hours, but for around 24 hours for proteins. A typical spectrometer is depicted schematically in Scheme33.

There are different methods of measuring the Mössbauer effect. The next picture shows the main principle of the experiment. A radioactive source is mounted onto a drive system. One measures as a function of velocity either the count rate of the transmitted radiation through the sample or the count rate of the backscattered electrons or gamma quanta.

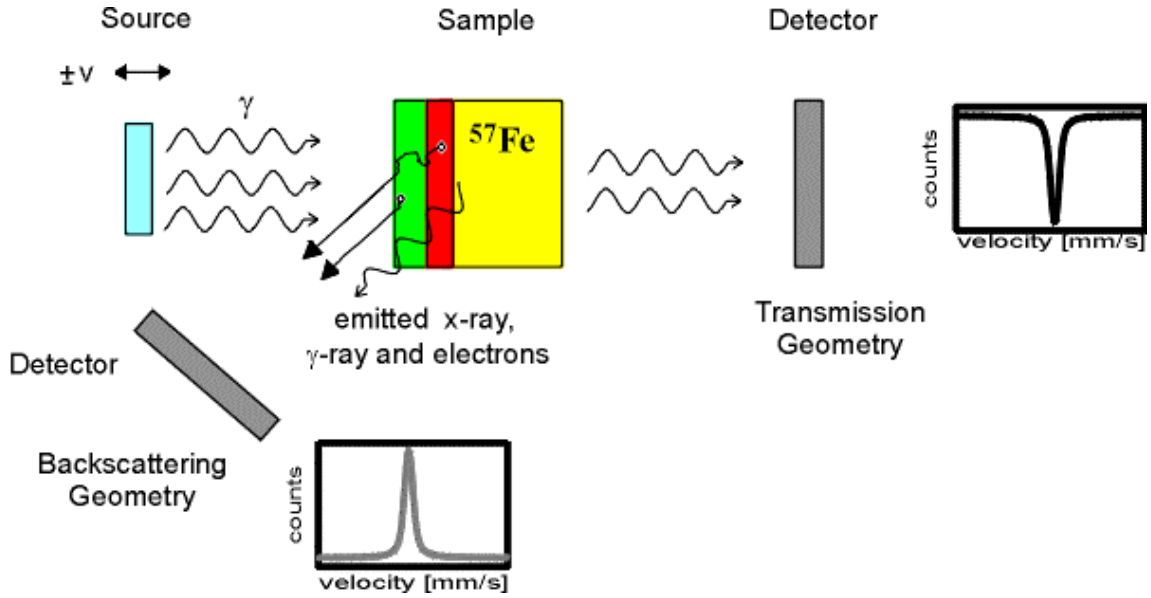

Scheme 33

Transmission Geometry is the standard Method. The experimental setup is very easy, but it is limited to powders or thin foils. The count rate decreases in resonance, because the radiation preferred can be absorbed. The whole sample contributes to the spectrum.

Backscattering Geometry measures either the emitted gamma or x-ray radiation or the emitted electrons. As this radiation has to leave the sample, only a layer at the surface contributes to the backscattered spectrum. The thickness of this layer depends on the range of the radiation. In the case of ^{57}Fe the gamma or x-rays have a range of approx. 10^{-6} m.

7.2.4.1 Mössbauer Spectroscopy.

Here we present some pictures of the Mossbauer equipment of the Department of Inorganic Chemistry at the University of Mainz (Laboratory of Prof. P. Gütlich) (Figure 69) where the measurements of this Thesis have been performed.

Figure 69. Moessbauer Spectrometer at the University of Mainz.

With this set\up it is also possible to irradiate the sample with a laser beam at different frequencies while measuring. Some interesting photo-induced phenomena may be observed.

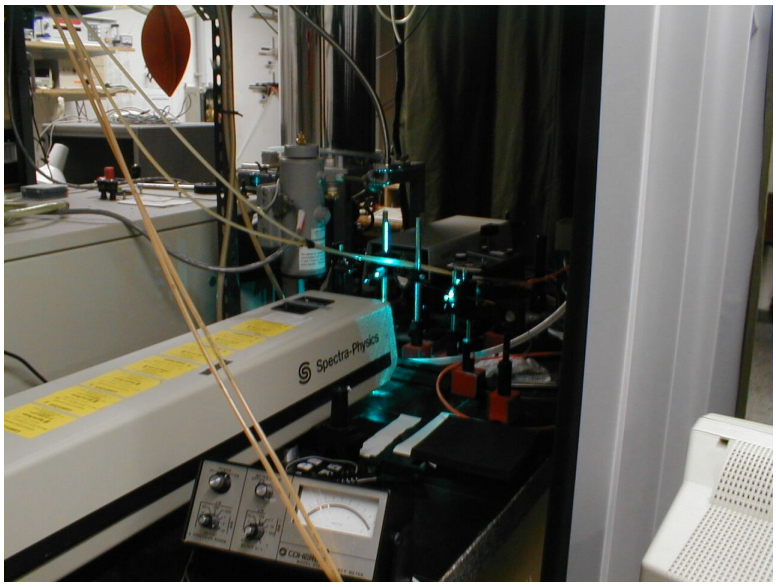

Figure 70. Laser coupled to the Moessbauer Spectrometer

REFERENCES

1. Cranshaw, T. E., Dale, B. W., Longworth, C. O. and Johnson, C. E. (**1985**) *Mössbauer Spectroscopy and its Applications*, Cambridge Univ. Press.
2. Debrunner, P. G. (**1993**) "*Mössbauer Spectroscopy of Iron Proteins*" in Biological Magnetic Resonance, 13, eds. Berliner, L. J. and Reuben, J., Plenum, New York, 59-101.
3. Edwards, P. R., Johnson, C. E. and Williams, R. J. P. (**1967**) "*Mössbauer Spectra of Some Tetrahedral Iron(II) Compounds*", *J. Chem. Phys*. *47*, 2074-2082.
4. Fraunfelder, H. (**1963**) The Mössbauer Effect, W. A. Benjamin, New York.
5. Greenwood, N. N. and Gibb, T. C. (**1971**) Mössbauer Spectroscopy, Chapman and Hall, London.
6. Huynh, B. H. and Kent, T. A. (**1984**) in Advances in Inorganic Biochemistry, eds. Eichhorn, G. L. and Luigi, G. M., Elsevier, New York, 163-223.
7. Lang, G., (1970) "Mössbauer Spectroscopy of Haem Proteins", Quart. Rev. Biophysics 3, I 1-60.
8. Lang, G. and Marshall, W. (**1966**) "*Mössbauer Effect in Some Hemoglobin Compounds*", Proc. Phys. Soc. 87, 3-34.
9. Long, G. J. and Stevens, J. G., eds. (**1986**) "*Industrial applications of the Mössbauer Effect*", Plenum Press, New York.
10. Mössbauer, R. (**1958**) "Kernresonzflureszenz von Gammastrahlung in Ir191", Z. Physik 151, 124-143
11. Thosar, B. V. and Iyengar, P. K., Eds. (**1982**) *Advances in Mössbauer Spectroscopy*, Elsevier, New York.
12. Varret, F. (**1976**) "*Crystal-Field Effects on High-Spin Ferrous Ion",* J. de Phsyique, Collogue CG, Supplement 12, Tome 37, 437-456.

7.3 | Nonlinear Optical Measurements

7.3.1. INTRODUCTION

Due to the lack of a simple experimental technique for the determintaion of the first hyperpolarizability β, there are considerable scatter in their reported values. Until recently EFISHG generation has been the standard technique to determine $\mu\beta_{vec}$ (the scalar product of the ground state dipole moment and the vectorial part of the first hyperpolarizability). However to obtain $\mu\beta_{vec}$ additional assumptions with regard to local field factors, second hyperpolarizability (γ) and symmetry must be imposed. Clays et al. introduced another method, Hyper-Rayleigh Scattering (HRS) technique, for measuring first hyperpolarizabilities. HRS provides the β value of a NLO chromophore relative to that of the pure solvent. For molecules of low symmetry, the different β tensor components can be readily determined form an analysis of the polarization of the HRS signal. Moreover since HRS, in contrast to EFISGH does not require a strong orienting electric field and therefore both apolar and ionic species can be evaluated.[1]

Since in this Thesis are presented results of NLO responses measured with HRS (β_{HRS}) and EFISHG (β_{EFISHG}) techniques, which moreover reveal a discrepancy between β_{HRS} and β_{EFISHG}, here we will present a small review for the requirements and the experimental set-up for both techniques.

7.3.2 HYPER-RAYLEIGH SCATTERING TECHNIQUE

HRS is an ideal technique for β measurements of nondipolar and/or ionic molecules, which are out of reach of the standard EFISHG technique. This method requires high peak-powder fundamental laser pulses and an efficient collection system of harmonic scattered photons.

Since second-order nonlinear effects are forbidden in the electric dipole approximation, the efficiency for Hyper-Rayleigh scattering in solution is fairly low. This is why the first reports of Hyper-Rayleigh scattering had to await the advent of megawatt peak power pulsed laser.[2] Theoretical aspects of the relevant mechanisms were discusses by

several authors.[3] The phenomenon has regained attention as a method for determining first hyperpolarizabilities of dissolved organic molecules without needing the recourse to superimposed dc fields or other means for producing preferential orientations.[4]

Although one of the conditions imposed upon quadratic nonlinear optical materials is noncentrosymmetry, second-harmonic generation has been observed in isotropic solutions. The potential of the HRS technique for the experimental determination of first hyperpolarizabilities is demonstrated with recently obtained results on molecules without dipole moment but with an octupolar charge distribution ionic species. The experimental aspects of Hyper-Rayleigh scattering in solution will be also discussed, with emphasis on the specific requirements imposed on the pulsed laser system.

Since centrosymmetric structures of molecules possessing a nonzero microscopic hyperpolarizability do not exhibit a macroscopic susceptibility , second harmonic generation is not allowed in centrosymmetric media. However, since in the liquid phase the lability of molecules is high, at a certain time t in a certain region of space r alignment of molecules can occur, breaking the centrosymmetry of the solution. On averaging, the symmetry of the liquid volume is conserved, but, due to the molecular rotational fluctuations, non-centrosymmetric regions are temporarily created that can exist in the duration of the incoming laser pulse, from where second harmonic generation can occur. However, this generation is incoherent. Second Harmonic photons are created and scattered in every direction, see Figure 71. This process is called Hyper Rayleigh scattering (HRS), referring to linear or Rayleigh scattering.

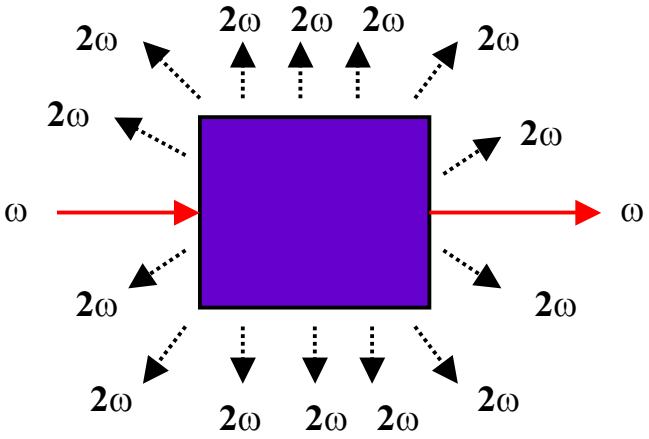

Figure 71. Scheme of HRS process in bulk liquid

For a two component solvent-solute system (e.g., *para*-nitroaniline in methanol), in which N_S and $\beta_{333,S}$, are the number density and the first hyperpolarizability of the solvent and N_s and $\beta_{333,s}$ the number density and the first hyperpolarizability of the solute, respectively. $S_J(2\omega)$ is written as

$$S_J(2\omega) = G_J B^2 I_Z^2 = G_J (N_S \beta_{333,S}^2 + N_s \beta_{333,s}^2) I_Z^2 \qquad \textbf{Equation 20}$$

For the low concentrations of solute used, the number density of the solvent N_S is approximately constant. Measurements of the second-harmonic scattered light intensity $S_J(2\omega)$ as a function of incident light intensity I_Z at different number densities of the solute N_s then show a linear dependence of the quadratic coefficients $G_J B^2$ on N_s, Figure 73 shows this linear dependence for the quadratic coefficients obtained form the data shown in Figure 72. From the intercept $G_J N_S \beta_S^2$ and the slope $G_J \beta_s^2$, β_s is calculated when β_S is known, or vice versa. Since no electric field directing the dipoles has to be applied, the local-field correction factor at zero frequency is eliminated.

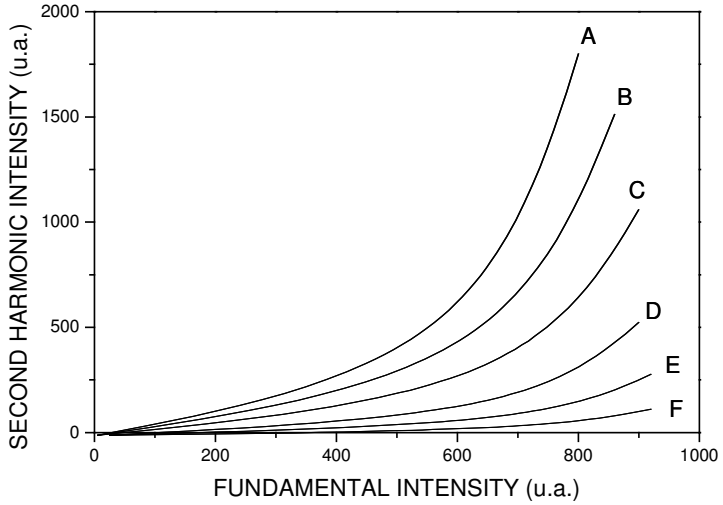

Figure 72. Hyper-Rayleigh scattering $S(2\omega)$ for *para*-nitroaniline in methanol at 293K at different number densities in units of 1018 cm^{-3}: (A) 92; (B) 46; (C) 23; (D) 9.2; (E) 4.6; (F) 1.8; the solid lines are fitted quadratic curves.

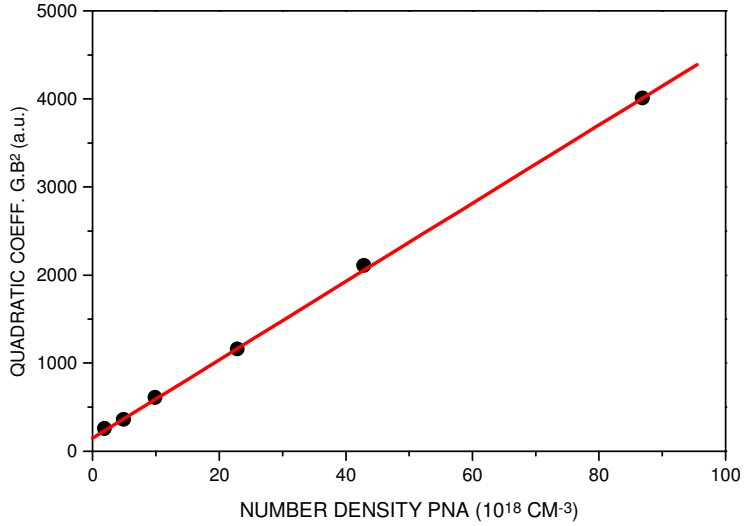

Figure 73. Quadratic coefficient GB^2 , obtained from the curves of Figure 72, as a function of number density of *para*-nitroaniline N_s ; the solid line is a linear fit.

7.3.2.1 Molecules Without Dipole Moment: Octupoles

The third-rank tensor β_{ijk} must conform to the symmetry of the molecule. As a consequence, for many symmetries, some of the elements of β_{ijk} will vanish and others will be required to have identical values. For equal frequencies of the exciting fields E_j and E_k, β_{ijk} must be symmetric in the second and third index j and k. If the imaginary parts of β_{ijk} vanish (no absorption in the frequency range ω_0 to $2\omega_0$), then β_{ijk} must be symmetric with respect to a permutation of all three indices (Kleinmann symmetry).[5] Under these conditions, β_{ijk} is a totally symmetric tensor, even for molecules lacking all symmetry operation except the identity operator. There are then at most 10 independent components. They consist of at most three dipolar (β_{111}, β_{222}, β_{333}) and at most seven octupolar contributions (β_{121}, β_{122}, β_{131}, β_{132}, β_{133}, β_{232} and β_{233}). As a result molecular symmetries excluding the dipolar but allowing octupolar contributions will still give rise to second-harmonic scattering.[6]

The classical molecular requirements for second-order NLO application have led to the design and optimisation of highly polarizable asymmetric organic molecules, typically asymmetrically *para* substituted polar benzene, azobenzene, stilbene derivatives and polyenes.[7] Octupolar molecules represent a new class of molecules that are potentially useful for NLO application, since these nonpolar molecules that are potentially useful for NLO properties with a strict cancellation of all vector-like observables, including the ground and excited state dipole moment. The advantages of using nonpolar species for NLO application include easier (noncentrosymmetric) crystallization, no dipolar interaction toward (centrosymmetric) aggregate formation, better ratio of off-diagonal versus diagonal tensor components and an improved efficiency-transparency trade-off. Based on these advantages, octupolar molecules are expected to become basic components of novel NLO materials.

Molecules with tetrahedral (T) or with D_{3h} symmetry belong to this class. Since they do not have a permanent dipole moment, they are not oriented by an electric field. It is therefore not possible to measure their hyperpolarizability by the usual EFISHG technique. The HRS technique is the only technique that makes the first hyperpolarizability tensor components of octupoles experimentally accessible.

7.3.2.2 Experimental Aspects of Hyper-Rayleigh Scattering in Solution

The experimental HRS apparatus that we used to measure the quadratic hyperpolarizabilities presented in Chapter 3.3 were performed in collaboration with the Centre de Physique Moléculaire Optique et Hetzienne of Bordeaux under the supervision of Dr. J. -F. Létard and Dr. E. Freysz.[8,9]

HRS has certain advantages over the electric field-induced second harmonic generation (EFISHG) techniques such as knowledge of the molecular dipole moment is not required and β values of charge and octupolar compounds may be measured. Measurements were made using a Q-switched Nd3+: YAG laser operating at 1064nm yielding a pulse of 10ns duration at 10Hz repetition rate. The incident pulse intensity is changed by a set composed of a computer controlled rotating half-wave plate followed by a Glan-Taylor

polarizer. The fundamental laser beam was focused on the centre of the 2cm path quarts cell with a long focal length plano-convex lens (f = 150mm)

The sample consists in an adequately designed spectrophotometric cell, presenting five-polished window so as to allow for simultaneous longitudinal illumination and transverse collection of the scattered emission. Solutions of increasing concentrations of the sample are preliminary cleaned through 0,5µm Millipore filters in order to remove most microscopic particles which could otherwise induce breakdowns in the presence of the focused laser beam.

The light scattered perpendicular of the incident beam was detected with a photomultiplier tube (PMT). A loss pass filter was used to filer out Rayleigh scattered infrared light. An interference filter (532nm central wavelength and 3nm transmission bandwidth) permitted a second harmonic detection. The electrical signal is first amplified then digitised by a lab-made box-car. The reference fundamental signal and harmonic signal photons detected by photomultiplier PMT tubes are processed by a lab-made box car, sampled and averaged, and then recorded on a XY table, giving $I^{2\omega}$ as a function of I^{ω}. The quadratic dependence of $I^{2\omega}$ versus I^{ω} is clearly evidence in Figure 72 for different concentrations of *p*-nitroaniline. The accuracy of our set-up on the determination of β was checked on a *p*-nitroaniline sample in methanol. The error is estimated to be approximately ± 15 %.

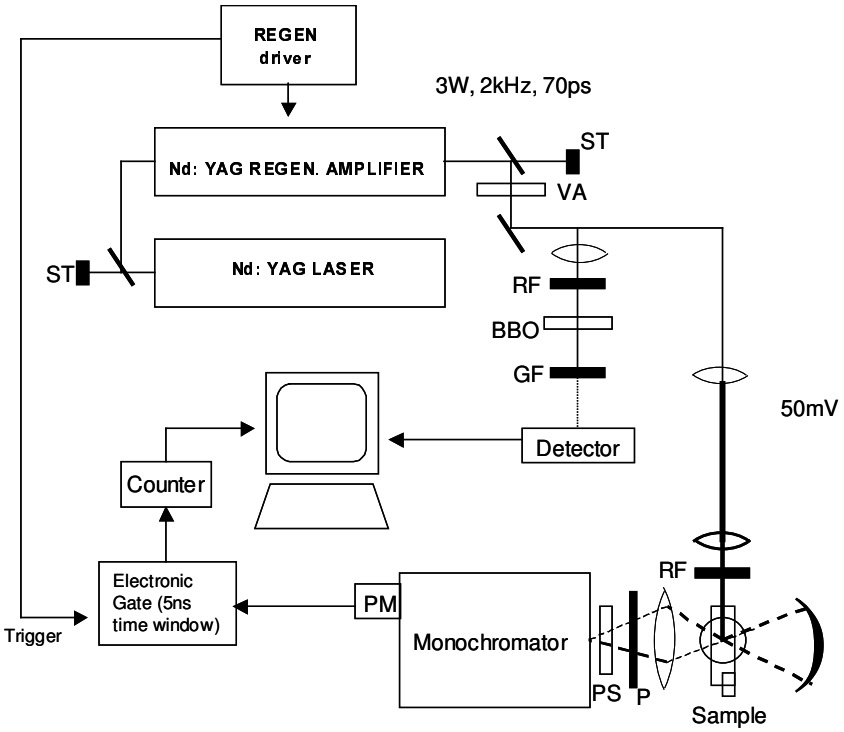

Figure 74. The experimental set-up for Hyper-Rayleigh scattering measurements where, VA: variable attenuator; RF: long wavelength pass filter; GF: short wavelength pass filter; P: polarizer; ST: beam stop; dashed lines: frequency doubled light.

The electric signal form the PMT is first amplified then digitalized by a lab-made box-car. The quadratic hyperpolarizability was derived form the intensity of the incoherent scattered light at 532nm according to Equation 22.

7.3.2.3 Laboratory and Molecular Reference Frame

The relation between the measured β^2 and the components of the molecular hyperpolarizability tensor in the molecular frame depends on the polarization state of the fundamental and harmonic beams, the experimental geometry and the molecule symmetry.

If the incident light is considered to propagate in the X direction with the polarization in the Z direction, the scattered light observed in the Y direction is given by:[10]

$$I_Z^{2\omega} = G\sum_s N_s \left\langle \beta_{ZZZ,s}^2 \right\rangle I_\omega^2 \qquad \textbf{Equation 21}$$

where *XYZ* indicates the laboratory coordinates and *Iz* or *Ix* is the HRS intensity, polarized respectively in the *Z* or *X* direction. If both polarizations are detected with equal sensitivity, then:

$$\left\langle \beta^2 \right\rangle = \left\langle \beta_{ZZZ}^2 \right\rangle + \left\langle \beta_{XZZ}^2 \right\rangle \qquad \textbf{Equation 22}$$

The HRS depolarization ratio is defined as:

$$\frac{I_X}{I_Z} = \frac{\left\langle \beta_{XZZ}^2 \right\rangle}{\left\langle \beta_{ZZZ}^2 \right\rangle} \qquad \textbf{Equation 23}$$

Assuming that the fundamental and harmonic frequencies are far from the material resonance frequency and that the HRS light is collected at 90° in the *Y* direction, the two hyperpolarizability tensor components of Equation 25 are given by:[11]

$$\beta_{ZZZ}^2 = \frac{1}{7}\sum_i \beta_{iii} + \frac{6}{35}\sum_{i,j} \beta_{iii}\beta_{ijj} + \frac{9}{35}\sum_i \beta_{ijj}^2 + \frac{6}{35}\sum_{i,j,k} \beta_{ijj}\beta_{ikk} + \frac{12}{35}\sum_i \beta_{ikj}^2 \qquad \textbf{Equation 24}$$

$$\beta_{XZZ}^2 = \frac{1}{35}\sum_i \beta_{iii} - \frac{2}{105}\sum_{i,j} \beta_{iii}\beta_{ijj} - \frac{11}{105}\sum_i \beta_{ijj}^2 - \frac{2}{105}\sum_{i,j,k} \beta_{ijj}\beta_{ikk} + \frac{8}{35}\sum_i \beta_{ikj}^2 \qquad \textbf{Equation 25}$$

where *ijk* indicates the molecular coordinates. The relations between the orientation averaged tensor components and the molecular hyperpolarizability tensor components were calculated by Bersohn *et al.*[12]

7.3.3 ELECTRIC FIELD SECOND INDUCED HARMONIC GENERATION TECHNIQUE

An EFISHG apparatus operating out of resonance at 1907nm was used to determine the β values of compound **3** and **5**. Such measurements were performed in the laboratory of Prof. Rafael Alcalá at the University of Zaragoza.

The measure of $\mu\beta$ with the EFISGH technique[13,14] is based on the measure of the intensity of the second harmonic wave (double frequency) due the interaction of an intense laser with oriented molecules with a centrosymmetry broken due to the application of a high electric field.

7.3.3.1 "Phase-Matching"

The condition required because a series of harmonic waves that propagate through materials were in phase interfering constructively and thus leading to a major efficiency of the conversion (fundamental beam→harmonic) is called Phase Matching. The origin of the "Phase-Mathcing", in the case of the second harmonic generation, is given by the intensity of its harmonic signal after passing the material of a given length **l**; and it is calculated with the following expression:[15]

$$I_{2\omega} \approx E^2{}_{2\omega} \approx \frac{1}{n^2{}_{\omega} - n^2{}_{2\omega}} \operatorname{sen}^2\left[\frac{l\omega(n_{\omega} - n_{2\omega})}{c}\right] \qquad \textbf{Equation 26}$$

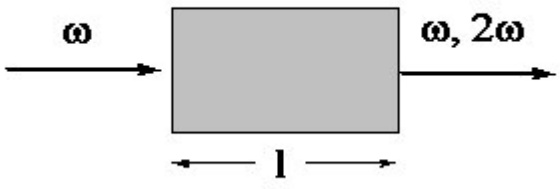

Figure 75. Generation of the second harmonic in a material of length **l**.

From this expression it can be deduced that in order to have the maximum efficiency in the conversion it is necessary that:

$n_\omega = n_{2\omega}$ and $2k_w = k_{2w}$ which is known as "Phase-matching"

But, it is impossible to have the phase-matching conditions. Then the intensity of the second harmonic is a periodic function of the length l giving place to the known **Maker Fringes** (Equation 26). EFISHG technique consists in the measure of the Maker Fringes in liquid samples by changing the length of the fundamental signal through the sample through a moving of the measure cell.

7.3.3.2 Light Source

Nd:YAG pulsed laser with Q.switch, model YG781C-10 of Quantel is used. The wavelength of the generated signal is 1064nm and it's energy of 1J/pulse. The frequency of repetition of the pulse 10 Hz. The system has a KDP crystal (potassium diacid phosphate, PO_4H_2K), that act as a frequency doubler and allow to have pulses of 570mJ and 532nm. In this way it is possible to have a great range of near infrared. Our measurements were all of them performed using configuration C. Here we show all possible configurations:

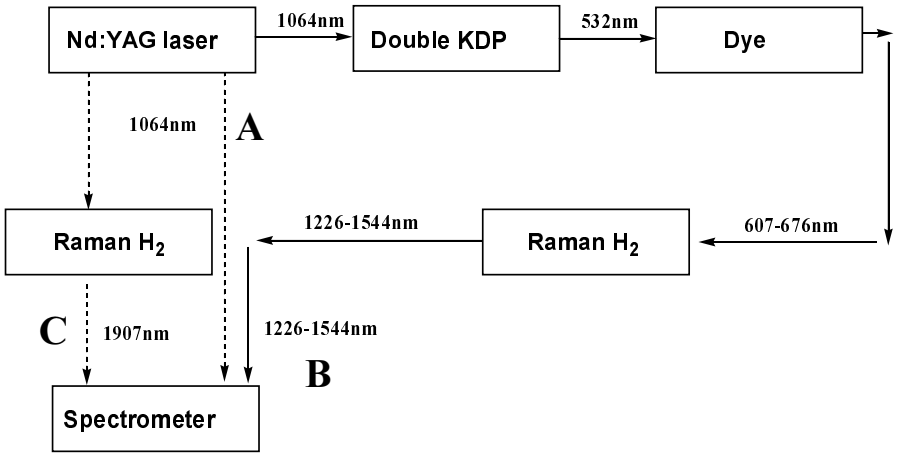

Figure 76. Diagram of the different experimental configurations, which are possible with the light source.

It is important to be able to change the incident wavelength in order to avoid absorption of light from the sample when it absorbs in the ω or 2ω region giving place to a high generation of the second harmonic but in this case due to resonant conditions.

In *Configuration C*: the 1064nm laser signal is lead to the Raman cell and the first Stoke is selected; 1907nm.

7.3.3.3 Nonlinear Optical Spectrometer

The spectrometer used in this Thesis is from the SOPRA Company. The following Figure shows the different parts of it:

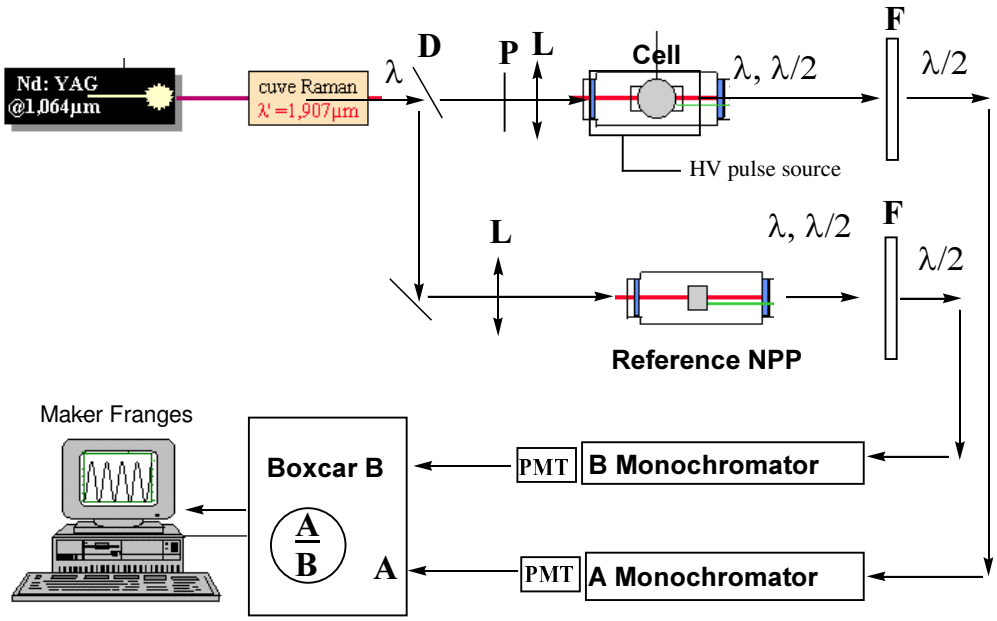

Figure 77. Scheme of the different parts of the spectrometer where; **P** Polaritzador. **L** Convergent lens **PMT** Photomultiplier **HV** High Voltage. **F** Filter. **D** Divisor.

Optical Elements: light form the source in partially reflected and divided in two beams. One of them takes 90% of the energy and it is lead to a Glan prism which allow the variation of the intensity of the resulting beam. Then a convergent lens focuses the laser signal in the measure cell. The other beam, with the 10% energy is focused to the reference NPP cell of N-(4-nitrophenil)-L-prolinol).

EFISHG cell: is shown in Figure 78 and it is constituted for two different parts: a) metallic cylinder with two quartz windows which contains the solution and b) two electrodes.

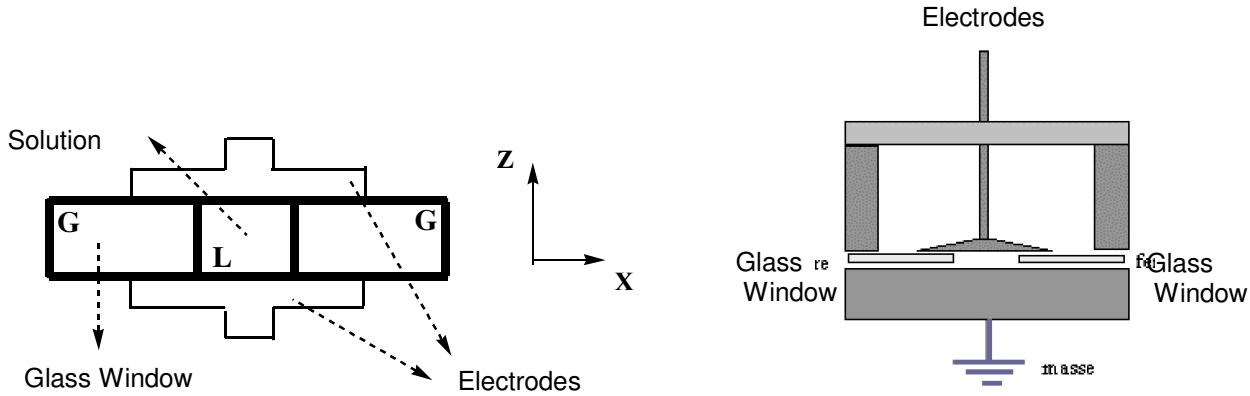

Figure 78. Scheme of the EFISHG cell, horizontal and vertical.

a) When the laser beam reach the solution inside the windows, the second harmonic generation is generated and it leaves the cell through the second window. As shown in Figure 78. the first and second window formed a little angle α of 1º-3,5º. Moving the cell along the Y direction, perpendicular to the incident beam, we can vary the distance that the incident beam go through the sample allowing the observation of Maker Fringes. Here we show an example of Maker Fringes obtained in a typical EFISHG measurement:

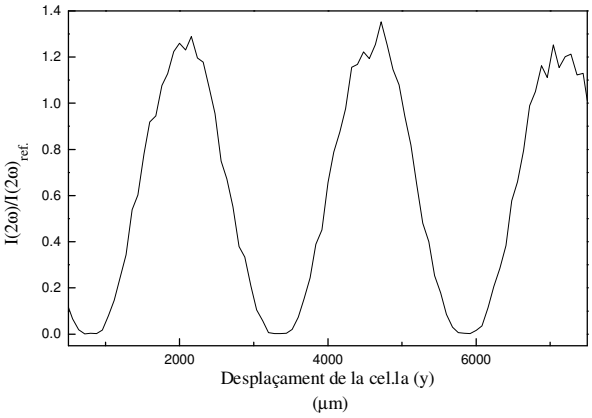

Figure 79. Maker Fringe obtained in methylene chloride using λ=1907nm.

From Equation 26 it is deduced that the period of Maker Fringes is proportional to the wavelength of the fundamental light.

b) The electrodes apply high voltage pulses synchronised with the laser pulses. The electric filed is perpendicular to the direction of propagation of the light, X. The voltage applied in our measurements is 7kV. The long filed pulses (10μs) in front of the short laser

pulses (6ns), allow considering a uniform electric field in the solution, which orient the molecules.

Detection System: The harmonic signal coming from the EFISGH cell and the signal coming from the reference cell are detected by a Photomultiplier (PM Hamamatsu, R2949). In order to minimize the laser instability during the measurement we make the quotient between the harmonic signal coming from the solution and the signal coming from the reference sample NPP.

7.3.3.4 Experimental Problems in β Determination

The main errors in EFISHG measurements are:

- Stability of the laser. Small deviations of the laser beam can suppose important deviations of the reproducibility of measurements. For that reason it is important to perform each measurement several times with different concentrations and measure the solvent before and after a series of measurements.
- Moreover, in some measurements there are other problems such as: absorption of the second harmonic generated, which makes necessary the use of new corrections in the calculation or modifications of the static field E_0 during the measurement due to the ionization of the sample. In the first case, it is better to avoid the absorption by changing the configuration of the light source (changing the fundamental wavelength) and in the second case it is better to use another solvent which doesn't dissociate the compound while measuring.

REFERENCES

1. Persoons, A.; Clays, K., Kauranen, M. Hendricks, E., Bijnens, W., *Synth. Met*. **1994**, *67*, 31.
2. (a) Terhune, R. W.; Maker, P. D.; Savage, C. M., *Phys. Rev. Lett.* **1965**, *14*, 681 (b) Weinberg, D. L.; *J. Chem. Phys,* **1967**, *47*,1307.
3. Giordmaine, J. A.; *Phys. Rev*., **1965**, *138*, 1599. (b) Kielich, S., *Chem. Phys. Lett.* **1967**, *1*, 441.
4. Clays, K.; persons, A*., Phys. Rev. Lett.* **1991**, *66*, 2980. (b) Clays, K.; Persoons, A., *Rev. Sce. Instrum.* **1992**, *63*, 3285.
5. Kleinman, D. A., *Phys, Rev.* **1962**, *126*, 1977.
6. Zyss, J., *Nonlinear Opt.* **1991**, *1*, 3.
7. Williams, D. J., *Angew. Chem. Int. Ed. Eng.* **1984**, *23*, 690.
8. Clays, K.; Persoons, A. *Rev. Sci. Instrum*. **1992**, *63*, 3285.
9. Hendrickx, E.; Clayus, K.; Personns, A., *Acc. Chem. Res.* **1998**, *31*, 675.
10. Verbiest, T.; et. Al., *Measurements of Molecular Hyperpolarizabilities using Hyper-Rayleigh Scattering, in Nonlinear Optical Properties of Organic Materials V*, D. J. Williams, Editor. **1992**, SPIE: Washington. p. 206.
11. Hendrickx, *et. al*., Hyper-Rayleigh Scattering in Isotropic Solution. *Acc. Chem. Res*., **1998**, *31*, 675.
12. Bersohn, R.; *et. al*. Double-Quantum Light Scattering by Molecules. *J. Chem. Phys*., **1966**, *45*(9), 3184
13. JL Oudar, and D.S. Chemla, *J. Chem. Phys*. **1977**, *66*, 2664.
14. Henry, rapport de DEA de physique de la matière condensée et des matériaux, université Louis Pasteur (**1990**)
15. J. Casas, "Òptica", **1985**, 297.

Abbreviations

A -	Acceptor
AFM -	Antiferromagnetic
BLA -	Bond alternation length
CCD -	Charge-Coupled Detector
CCDC -	Crystallographic Data Center Cambridge
Cp	Ciclopentadiene
CPU -	Computerized Processes Unlimited
CS -	Charge Separation
D -	Donor
EFISHG-	Electron Field Induced Second Harmonic Generation
EPR -	Electron Paramagnetic Resonance
ET -	Electron Transfer
FIM -	Ferrimagnetic
FM -	Ferromagnetic
HOMO -	Highest Occupied Molecular Orbital
HPLC-	High Pressure Liquid Chromatograghy
HRS -	Hyper Rayleigh Scatter
IET-	Intramolecular Electron Transfer
IR-	Infrared
IT -	Intervalence Transfer
IVB-	Intervalence Transfer Band
LMCT -	Ligand to Metal Charge Transfer
LSER -	Linear Solvation Energy Relationship
LUMO -	Lowest Occupied Molecular Orbital
MALDI-TOF-	(Matrix Assisted) Desorption Ionization-Time of Flight
NIR -	Near Infrared
MLCT -	Metal to Ligand Charge Transfer
NLO -	Nonlinear Optics
MM -	Molecular Materials
NMR -	Nuclear Magnetic Resonance
PCB -	Pentachlorobenzene
PMT -	Photomultiplier Tube
PTM -	Polychlorotriphenylmethyl
SHG -	Second Harmonic Generation
SOMO -	Single Occupied Molecular Orbital
SONLO-	Second order Nonlinear Optics
SQUID -	Superconducting Quantum Interference Device
TCB -	Trichlorobenzene
TEA -	Triethylammine
TIP -	Temperature Independent Paramagnetism
TTM -	Trichlorotriphenylmethyl
UV	Ultraviolet
WFM -	Weak Ferromagnetic
ZINDO	Zerner Intermediate Neglect of Differential Overlap

8 | Publications

Papers revised by the Doctoral Commission

Papers after the Doctoral Commission

Paper I

I. **A new Photomagnetic Molecular System Based on Photoinduced Self-Assembly of Radicals**
I.Ratera, D. Ruiz-Molina, J. Vidal-Gancedo, K. Wurst, Nathalie Daro, J.-F. Létard, C. Rovira, J. Veciana

Angew. Chem. Int. Ed. Engl. **2001***, 40, No.5,* 919

Paper II

II. **Formation of a Biradical Species from a Monoradical with a Photoisomerizable Imine Group**

D. Ruiz-Molina, I. Ratera, J. Vidal-Gancedo, N. Daro, J.-F. Létard, C. Rovira, J. Veciana

Synthetic Metals, **2001**, *121,* 1804.

Paper III

III. **EPR Study of the *cis* and *trans* Isomers of a Ferrocenyl Schiff-Base Polychlorotriphenylmethyl Radical**
I.Ratera, D. Ruiz-Moina, J. Vidal-Gancedo, C. Rovira, J. Veciana,

Polyhedron, **2001***, 20 (11-14)* 1643-1645.

Paper IV

IV. **Ferrocene as a Ferromagnetic Coupler. Synthesis and Characterization of a Ferrocene Bridged Polychlorotriphenylmethyl Diradical**
O. Elsner, D. Ruiz-Molina, I. Ratera, J. Vidal-Gancedo, C. Rovira, J. Veciana,

J. Organomet. Chem., **2001***, (637-639),* 252-257

Paper V

V. **Nonlinear Optical Properties of a New Stable Ferrocenyl Schiff-base Polychlorotriphenylmethyl Radical**
I.Ratera, D. Ruiz-Molina, C. Sánchez, R. Alcalá, C. Rovira, J. Veciana, ,

Synthetic Metals, **2001***, 121,* 1834.

Paper VI

VI. **Non Linear Optical properties of Polychlorotriphenylmethyl Radicals. Towards the Design of "Super-Octupolar" Molecules**
I.Ratera, J.-F. Létard, S. Marcén, D. Ruiz-Molina, E. Freysz, C. Rovira, J. Veciana

Chem. Phys. Lett., **2002,** *363,* 245-251

Paper VII

VII. Intramolecular Electron Transfer in Organic Molecules. Molecular Nanowires.

D. Ruiz-Molina, J. Vidal-Gancedo, J. Sedó, I. Ratera, J. Veciana and C. Rovira
Molecular Low Dimensional and Nanostructured Materials for Advanced Applications (MMAA), p.125-138. Edited by A. Graja, B. R. Bulka and F. Kajzar. NATO ASI Series, II. Mathematic, Physics and Chemistry, ISBN 1-4020-0578-4, Vol. 59, **2002**